

# Turbine Blade Heat Transfer Calculations Using Two-Equation Turbulence Models

Jonas Larsson

jola@tfd.chalmers.se

Thermo and Fluid Dynamics

Chalmers University of Technology

S-412 96 Gothenburg, Sweden

## Abstract

*A full Navier-Stokes solver is used to calculate external heat-transfer in two linear two-dimensional turbine cascades, one subsonic and one transonic. Heat-transfer results obtained with two low-Re  $k - \epsilon$  models (Chien and Launder-Sharma) and two  $k - \omega$  models (Wilcox standard and transition) are compared with measurements. Good agreement is found in some regions, but the suction-side transition and the leading-edge is not predicted correctly. Problems with too high turbulence levels in the leading edge region are investigated. The numerical quality of the results is investigated, and a few general guidelines about the numerics are given. Grid and scheme independence is also demonstrated.*

## Nomenclature

$C_p$	Specific heat [J/kgK]
$e$	Internal energy [J/kg]
$e_0$	Total energy [J/kg]
$k$	Turbulent kinetic energy [J/kg]
$p$	Static pressure [Pa]
$Pr$	Prandtl number []
$q_i$	Heat flux [W/m <sup>2</sup> ]
$t$	Time [s]
$T$	Static temperature [K]
$u_i$	Velocity [m/s]
$u^*$	Friction velocity [m/s]
$Y^+$	Non-dim. distance from wall = $\frac{u^* y}{\nu}$ []
$\gamma$	Specific heat ratio = $C_p/C_v$ []
$\epsilon$	Dissipation of $k$ [J/kg s]
$\delta_{ij}$	Kronecker's delta function []
$\mu$	Dynamic viscosity [Ns/m <sup>2</sup> ]
$\nu$	Kinematic viscosity [m <sup>2</sup> /s]
$\rho$	Density [kg/m <sup>3</sup> ]
$\tau_{ij}$	Shear stress tensor [N/m <sup>2</sup> ]
$\omega$	Specific dissipation [s <sup>-1</sup> ]

<b>Subscript:</b>	$t$	Turbulent property
<b>Superscript:</b>	$diff$	Diffusive part
	$conv$	Convective part
	$lam$	Laminar part
	$tot$	Laminar+turbulent part
	$turb$	Turbulent part
	$turb$	Turbulent part
	'	Reynolds fluctuating part
	"	Favre fluctuating part
	$\bar{\cdot}$	Reynolds average
	$\tilde{\cdot}$	Favre average

## 1 Introduction

The objective of this paper is to present results and experience from turbine heat-transfer calculations using two-equation turbulence models in a modern full Navier-Stokes code.

The heat-loads in a turbine are very important. A good design from a thermal point of view might allow a higher inlet temperature, less cooling or a lighter design, thus increasing the performance or efficiency of the machine. A method to predict the heat-loads in the design phase of a turbine would be a very valuable engineering tool.

The external heat-transfer in a turbine is influenced by many parameters, and detailed information about the flow is needed in order to obtain good results. The flow is characterized by regions with large continuous pressure gradients, causing strong acceleration and deceleration. Under certain operating conditions there might be separated regions. Some turbines operate under transonic conditions, and shocks, which interact with the boundary layers, can influence the heat-transfer. The mass-flow into the turbine comes from a combustor, and is strongly turbulent. This causes an early boundary-layer transition, and an increased heat-transfer in both the laminar [11] and the turbulent parts [24] [19]. Multi-staging gives rise to wakes and shocks from the preceding stages, which

sweep over the blades. As shown by many authors [3] [10] [12] [20] [23] this can increase the heat-transfer significantly, although a high inlet turbulence level tends to decrease the relative importance of this effect. In a real turbine three-dimensional effects can also be important for the heat-transfer [4]. If the blades are film-cooled this leads to even more complications, and this will not be considered here.

Clearly it is a very formidable task to predict heat-transfer in this kind of turbines. Several features of the global flow-field are closely coupled to the boundary-layers and the heat-transfer. All calculations presented here are for stationary and two-dimensional turbine cascades without cooling. This greatly simplifies the numerical analysis, and makes it possible to efficiently test different turbulence models, and study the influence of other important factors. In the future, when faster computers are available, the methods can easily be extended to unsteady and three-dimensional cases. The main principles used are the same, but the amount of calculation work necessary to obtain a solution is several orders of magnitudes greater. The test-cases chosen here are a subsonic cascade by Nicholson et. al. [21], and a highly loaded transonic cascade [2] from the von Karman Institute for Fluid Dynamics. Other similar cases, which were also considered, can be found in [14] and [30].

There are several different ways to calculate external heat-transfer in a turbine cascade. Classical methods like boundary layer solvers and Navier-Stokes solvers with algebraic turbulence models have been used by many researchers in the past [5], [1], [9]. These methods are efficient, and can sometimes give good results. However, there are big problems with separated regions, shocks and high inlet turbulence levels. With a transport model these problems can be solved, or at least reduced.

Using two-equation turbulence models in a turbine cascade simulation introduces several new problems. Many of these models behave badly in the stagnation region around the leading edge, and in order to obtain good results it is necessary to do something about this. Two-equation turbulence models can also predict by-pass transition, but as shown below this is very difficult in a turbine simulation.

## 2 Governing Equations

The governing equations are the Favre averaged [13] continuity equation (1), momentum equation (2) and energy equation (3). Reference [27] and [25] contains an overview of the turbulent equations governing compressible flow. For a detailed description of the main

assumption underlying the equations as used here see [16]. By assuming that the fluid is a perfect gas the pressure,  $\bar{p}$ , is given by (10).

All turbulence models used in this work rely on the Boussinesq's assumption - that the principal axes of the Reynolds stress tensor are coincident with those of the mean strain-rate tensor. This makes it possible to express the total shear stresses as a sum of the laminar and the turbulent contribution (4). The laminar part is given directly by (5), and the turbulent part is estimated with an effective eddy-viscosity,  $\mu_t$ , as in (6). The eddy-viscosity is then calculated with a separate turbulence model (see below).

The heat-flux,  $q_i$ , is treated in a similar way, according to Reynolds analogy. First the heat-flux,  $q_i$ , is divided into a laminar and a turbulent part (7). The laminar part,  $q_i^{lam}$ , is given directly by (8). To model the turbulent heat-flux a constant turbulent Prandtl number,  $Pr_t = 0.9$ , is assumed, and (9) then gives an approximation of the heat-flux generated by turbulent fluctuations. The use of a constant turbulent Prandtl number is not self-evident. However, other researchers [5] have reported no significant difference in heat transfer predictions when using an algebraic expression for the turbulent Prandtl number instead of a constant value.

It should be noted that for historical reasons the turbulent transport and molecular diffusion of turbulent energy have been neglected in the energy equation (3). This does not influence the results at all for the subsonic and transonic cases presented here.

$$\frac{\partial \bar{p}}{\partial t} + \frac{\partial}{\partial x_i} [\bar{\rho} \tilde{u}_i] = 0 \quad (1)$$

$$\frac{\partial}{\partial t} (\bar{\rho} \tilde{u}_i) + \frac{\partial}{\partial x_j} [\bar{\rho} \tilde{u}_j \tilde{u}_i + \bar{p} \delta_{ij} - \tau_{ij}^{tot}] = 0 \quad (2)$$

$$\frac{\partial}{\partial t} (\bar{\rho} \tilde{e}_0) + \frac{\partial}{\partial x_j} [\bar{\rho} \tilde{u}_j \tilde{e}_0 + \tilde{u}_j \bar{p} + \tilde{q}_j^{tot} - \tilde{u}_i \tau_{ij}^{tot}] = 0 \quad (3)$$

Where

$$\tau_{ij}^{tot} \stackrel{def}{=} \tau_{ij}^{lam} + \tau_{ij}^{turb} \quad (4)$$

$$\tau_{ij}^{lam} = \mu \left( \frac{\partial \tilde{u}_i}{\partial x_j} + \frac{\partial \tilde{u}_j}{\partial x_i} - \frac{2}{3} \frac{\partial \tilde{u}_k}{\partial x_k} \delta_{ij} \right) \quad (5)$$

$$\begin{aligned} \tau_{ij}^{turb} &\stackrel{def}{=} -\overline{\rho u_i'' u_j''} \approx \\ &\approx \mu_t \left( \frac{\partial \tilde{u}_i}{\partial x_j} + \frac{\partial \tilde{u}_j}{\partial x_i} - \frac{2}{3} \frac{\partial \tilde{u}_k}{\partial x_k} \delta_{ij} \right) - \frac{2}{3} \bar{p} k \delta_{ij} \quad (6) \end{aligned}$$

$$\tilde{q}_j^{tot} \stackrel{def}{=} \tilde{q}_j^{lam} + \tilde{q}_j^{turb} \quad (7)$$

$$\widetilde{q}_j^{lam} \approx -C_p \frac{\mu}{Pr} \frac{\partial \widetilde{T}}{\partial x_j} = -\frac{\gamma}{\gamma-1} \frac{\mu}{Pr} \frac{\partial}{\partial x_j} \left[ \frac{\overline{p}}{\rho} \right] \quad (8)$$

$$\mu_t = C_\mu f_\mu \rho \frac{k^2}{\epsilon} \quad (13)$$

$$\begin{aligned} \widetilde{q}_j^{turb} \stackrel{def}{=} C_p \overline{\rho u_j'' T''} &\approx -C_p \frac{\mu_t}{Pr_t} \frac{\partial \widetilde{T}}{\partial x_j} = \\ &= -\frac{\gamma}{\gamma-1} \frac{\mu_t}{Pr_t} \frac{\partial}{\partial x_j} \left[ \frac{\overline{p}}{\rho} \right] \end{aligned} \quad (9)$$

$$P = \tau_{ij}^{turb} \frac{\partial u_i}{\partial x_j} \quad (14)$$

$$\overline{p} = (\gamma-1) \overline{\rho} \left( \widetilde{e}_0 - \frac{\widetilde{u}_k \widetilde{u}_k}{2} - k \right) \quad (10)$$

## 2.1 Turbulence Models

The turbulence models were chosen in order to give a good representation of well established two-equation models. Future work will cover more recent and advanced models. The models chosen are the low-Reynolds  $k - \epsilon$  models of Chien [6] and Launder-Sharma [18], and two  $k - \omega$  models by Wilcox, one standard version [26] without any near-wall modifications, and one transition version [28], specifically optimized for transition simulations. Wilcox's book [27] contains an exhaustive presentation of the  $k - \omega$  models. A good review of classical low-Re  $k - \epsilon$  models can be found in [22].

None of these models have been specifically developed for compressible flow calculations. The only compressible modification used here is that the turbulence equations are written in a conservative formulation. For the cases presented here this is sufficient.

All of the models were tested on simple flat-plate benchmark problems to assure a correct implementation before using them in cascade simulations.

### 2.1.1 Low-Re $k - \epsilon$ Models

The low-Re  $k - \epsilon$  models can be written in the general form of equation (11), (12), (13) and (14).  $C_{\epsilon_1}$ ,  $C_{\epsilon_2}$ ,  $C_\mu$ ,  $\sigma_k$  and  $\sigma_\epsilon$  are model constants. The damping functions  $f_\mu$ ,  $f_1$  and  $f_2$  and the extra source terms  $D$  and  $E$  are only active close to solid walls and make it possible to solve  $k$  and  $\epsilon$  down to the viscous sublayer. Table 1 summarizes the constants, damping functions and boundary conditions for all  $k - \epsilon$  models used.

$$\frac{\partial}{\partial t} (\rho k) + \frac{\partial}{\partial x_j} \left[ \rho k u_j - \left( \mu + \frac{\mu_t}{\sigma_k} \right) \frac{\partial k}{\partial x_j} \right] = P - \rho \epsilon - \rho D \quad (11)$$

$$\begin{aligned} \frac{\partial}{\partial t} (\rho \epsilon) + \frac{\partial}{\partial x_j} \left[ \rho \epsilon u_j - \left( \mu + \frac{\mu_t}{\sigma_\epsilon} \right) \frac{\partial \epsilon}{\partial x_j} \right] = \\ = (C_{\epsilon_1} f_1 P - C_{\epsilon_2} f_2 \rho \epsilon) \frac{\epsilon}{k} + \rho E \end{aligned} \quad (12)$$

	<i>Chien</i>	<i>Launder-Sharma</i>
$c_\mu$	0.09	0.09
$\sigma_k$	1	1
$\sigma_\epsilon$	1.3	1.3
$D$	$2\nu \frac{k}{y^2}$	$2\nu \left( \frac{\partial \sqrt{k}}{\partial y} \right)^2$
$E$	$-\frac{2\nu\epsilon}{y^2} e^{-0.5y^+}$	$2\nu\nu_t \left( \frac{\partial^2 u}{\partial y^2} \right)^2$
$C_{\epsilon_1}$	1.35	1.44
$C_{\epsilon_2}$	1.8	1.92
$f_\mu$	$1 - e^{-0.0115y^+}$	$1 - e^{\frac{-3.4}{(1+Re_t/50)^2}}$
$f_1$	1	1
$f_2$	$1 - 0.22e^{-\left(\frac{Re_t}{6}\right)^2}$	$1 - 0.3e^{-Re_t^2}$
$y^+ \stackrel{def}{=} \frac{yu^*}{\nu}$ , $Re_t \stackrel{def}{=} \frac{k^2}{\nu\epsilon}$ , $k_{wall} = 0$ , $\epsilon_{wall} = 0$		

Table 1: Model Parameters, Low-Re  $k - \epsilon$  Models

### 2.1.2 $k - \omega$ Models

The  $k - \omega$  models can be written in the general form of equation (15), (16), (17) and (18). The model parameters for the two models used are given in table 2.

$$\frac{\partial}{\partial t} (\rho k) + \frac{\partial}{\partial x_j} \left[ \rho u_j k - (\mu + \sigma^* \mu_t) \frac{\partial k}{\partial x_j} \right] = P - \beta^* \rho \omega k \quad (15)$$

$$\frac{\partial}{\partial t} (\rho \omega) + \frac{\partial}{\partial x_j} \left[ \rho u_j \omega - (\mu + \sigma \mu_t) \frac{\partial \omega}{\partial x_j} \right] = \alpha \frac{\omega}{k} P - \beta \rho \omega^2 \quad (16)$$

$$\mu_t = \alpha^* \frac{\rho k}{\omega} \quad (17)$$

$$P = \tau_{ij}^{turb} \frac{\partial u_i}{\partial x_j} \quad (18)$$

The asymptotic behavior of  $\omega$  approaching a wall is that  $\omega \sim 1/y^2$  as  $y \rightarrow 0$ . However, using a finite value of  $\omega_{wall}$  is good from a numerical point of view, and this is also what Wilcox recommends [27]. The

	<i>Standard Version</i>	<i>Transition Version</i>
$\alpha^*$	1	$\frac{\alpha_0^+ + (Re_t/R_k)}{1 + (Re_t/R_k)}$
$\alpha$	$\frac{5}{9}$	$\frac{5}{9} \cdot \frac{\alpha_0^+ + (Re_t/R_w)}{1 + (Re_t/R_w)} \cdot \frac{1}{\alpha^*}$
$\beta^*$	$\frac{9}{100}$	$\frac{9}{100} \cdot \frac{\frac{5}{18} + (Re_t/R_\beta)^4}{1 + (Re_t/R_\beta)^4}$
$\beta$	$\frac{3}{40}$	$\frac{3}{40}$
$\sigma^*$	$\frac{1}{2}$	$\frac{1}{2}$
$\sigma$	$\frac{1}{2}$	$\frac{1}{2}$
$Re_t \stackrel{def}{=} \frac{\rho k}{\omega \mu}$ $\alpha_0^* = \frac{\beta}{3}$ $\alpha_0 = \frac{1}{10}$ $R_\beta = 8$ $R_k = 6$ $R_w = 2.7$		

Table 2: Model Parameters, Wilcox  $k - \omega$  Models

surface roughness model gives a finite value for  $\omega_{wall}$  as in equation (19) and (20). If  $k_R^+$ , which is the non-dimensional average sand-grain roughness height, is set to a value below 5 a hydraulically smooth surface is obtained. If not otherwise stated, a  $k_R^+$  value of 5 has been used in all simulations presented here.

$$\omega_{wall} = \frac{u^{*2}}{\nu} S_R \quad (19)$$

Where

$$S_R = \begin{cases} (50/k_R^+)^2 & k_R^+ < 25 \\ 100/k_R^+ & k_R^+ \geq 25 \end{cases} \quad k_R^+ \stackrel{def}{=} \frac{u^* k_R}{\nu} \quad (20)$$

### 3 Numerical Method

In short the numerical method is an explicit three-stage Runge-Kutta time-marching method using an optimized local time-step. The grid is a structured multi-block grid, which is generated with transfinite interpolation. The convective (Euler) parts are discretized with a third order accurate cell-centered finite volume reconstruction scheme with upwind-biasing based on the characteristic variables and associated velocities. For the turbulent quantities ( $k$  and  $\epsilon/\omega$ ) a TVD limiter has to be added to the third order scheme, making it second order accurate. The viscous parts are discretized with a compact second order scheme.

The use of an explicit method and a local time-step makes it a bit difficult to solve  $k$  and  $\epsilon/\omega$ . Especially at the beginning of a simulation stability problems can occur, and it might be necessary to temporarily limit the turbulent viscosity, use a first order upwind scheme for  $k$  and  $\epsilon/\omega$  or limit the time-step locally to

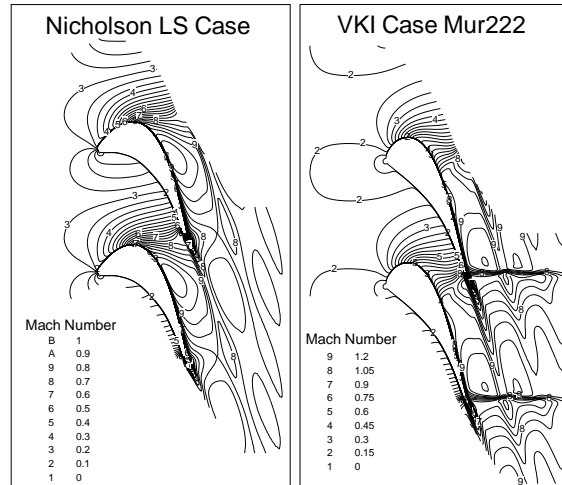


Figure 1: Mach Number Contours

avoid too large relative cell-updates. After a few thousand time-steps all of these modifications can usually be removed.

At the inlet and outlet the simplest type of absorbing boundary conditions are used. The same upwind-biased characteristic reconstruction scheme, which is used in the domain, is also used at the inlet and outlet boundaries. At the blade surface the flow variables are mirrored to ghost-cells outside the domain to get the correct conditions at the wall.

A more thorough description of the numerical methods used can be found in [16].

## 4 Simulations

Figure 1 shows Mach number contours for the two cascades. It should be pointed out that for both these cases all turbulence models give almost exactly the same Mach number and pressure distribution on the blade surface. Differences seen in the heat-transfer is thus not caused by differences in the global flow field, but is a result of details in the boundary-layers or the turbulent fields. Further details about the flow in these cascades are given below.

Details about the inlet and outlet conditions and geometrical data for the cascades are given in the references [21] and [2]. The turbulent length scale ( $L = k^{1.5}/\epsilon = \sqrt{k}/(\beta^*\omega)$ ) at the inlet is often not known, and if not otherwise stated a length corresponding to 10% of the pitch was used.

### 4.1 Subsonic Cascade

The subsonic case is a “low-staggered” cascade, herein referred to as “LS”. Heat-transfer measurements of

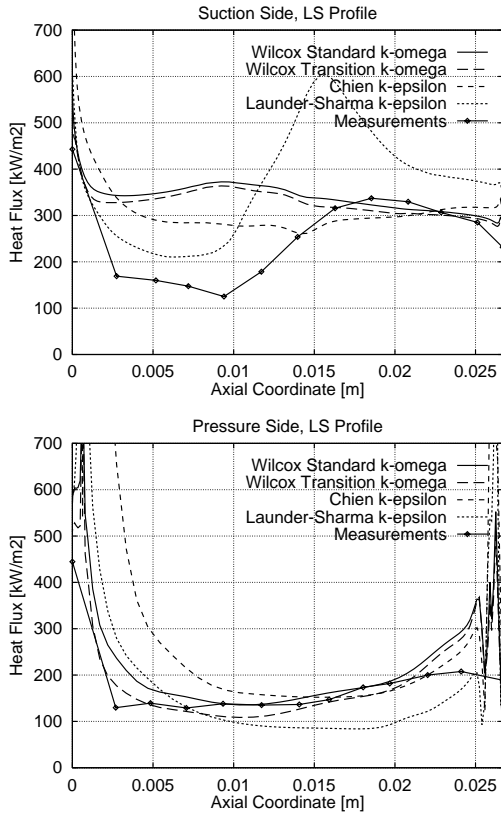


Figure 2: Heat Transfer, Subsonic LS Profile,  $Tu=4\%$

this cascade, at several different operating conditions, are available in Nicholson et. al. [21]. The conditions used here is the high turbulence level (4%) at design flow-rate, which gives a maximum Mach number just below 1 and a Reynolds number based on exit velocity and chord of  $1.113 \cdot 10^6$ . On the suction side the boundary layer is laminar up 30% of the axial distance, where transition starts. The transition region is quite long, and at about 60% of the axial distance the boundary layer has become fully turbulent. On the pressure side transition occurs close to the leading edge, and the boundary layer remains in a turbulent state over the whole blade. The acceleration at the rear of the blade does not cause any relaminarization.

In a previous paper [17] the low turbulence version ( $< 0.2\%$ ) of this case were simulated with an algebraic turbulence model (Baldwin-Lomax). The results obtained were very good. However, in order to model the influence of a higher inlet turbulence level, only two-equation models are used for the high turbulence cases presented here.

Figure 2 shows heat transfer results obtained with all four two-equation models. On the suction surface only the Launder-Sharma model is able to capture the laminar region. All other models predict an almost

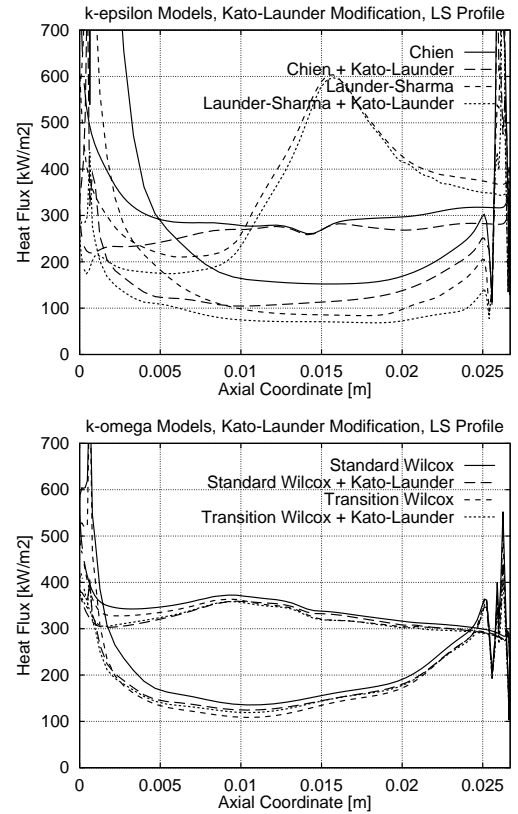


Figure 3: Influence of Kato-Launder Modification

immediate transition, and a fully turbulent boundary layer over the whole suction side. The Launder-Sharma model predicts a too abrupt transition, and a big overshoot in the heat transfer. The final heat transfer in the fully turbulent region is also a bit too high. The other three models predict the heat transfer in the turbulent region on the suction side very well.

On the pressure side all models give quite good results. The Launder-Sharma model gives a bit too low results in the downstream half of the blade, but the three other models are very close to the measurements. All models have some problems close to the trailing edge, where the acceleration of the flow is quite strong. It looks as if the laminarizing effect of this acceleration was not captured correctly by the turbulence models. There are also some oscillations at the trailing edge, which are very difficult to avoid.

The  $k - \epsilon$  models, especially the Chien model, predicts a high peak in the heat transfer at the leading edge. This peak is also visible with the  $k - \omega$  models, but it is substantially smaller.

#### 4.1.1 Problems at the Leading Edge

All models used here predict too high turbulence levels around the leading edge. This can affect the heat-transfer significantly. The excessive production is caused by the large normal strains present in the stagnation region. The Boussinesq assumption is not valid in this kind of flows, and predicts far too high production of  $k$ . A simple way to test how this affects the results is to modify the production term,  $P$ , in equation (14) and (18) in the following way:

$$\begin{aligned} P &= C_\mu \rho \epsilon S \Omega \\ S &= \frac{k}{\epsilon} \sqrt{\frac{1}{2} \left( \frac{\partial u_i}{\partial x_j} + \frac{\partial u_j}{\partial x_i} \right)^2} \\ \Omega &= \frac{k}{\epsilon} \sqrt{\frac{1}{2} \left( \frac{\partial u_i}{\partial x_j} - \frac{\partial u_j}{\partial x_i} \right)^2} \end{aligned} \quad (21)$$

This modification, originally suggested by Kato and Launder [15], turns off the production of  $k$  in irrotational flows. The flow in the stagnation region is nearly irrotational, and thus the turbulence level is significantly reduced in this region. Figure 3 shows heat-transfer results obtained with and without this modification. All models give significantly lower heat transfer in the stagnation point with this modification. The results with the  $k-\omega$  models are a bit lower than the measurements, as can be expected since the production term is essentially removed with the Kato-Launder modification. The Chien model, however, still has a small peak at the stagnation point. This is probably caused by the fact that the  $\epsilon$  equation has a tendency to convect too large length-scales into the boundary layer in stagnation flows. Using an extra source term in the  $\epsilon$  equation in order to reduce the departure from the equilibrium length-scale, as suggested by Yap [29], also removes this peak [17]. The Launder-Sharma models seems to be less affected by this problem, and for this particular case it is not necessary to use the Yap correction with this model. The  $k-\omega$  models do not have this problem at all.

The Kato-Launder modification only affects the  $k-\omega$  models in the stagnation point, whereas the  $k-\epsilon$  models give lower heat-transfer over the entire pressure side. This indicates that the effect of the modified production term is important also in the  $\epsilon$  equation.

The author does not recommend using the Kato-Launder modification. It was used here only in order to demonstrate which effect the problem with too high production of turbulent energy in flows with large normal strain has. The Kato-Launder model reduces the production of turbulent energy too much, and can

sometimes give bad results on the pressure side. Instead of using this kind of ad-hoc modification to alleviate the problems with the Boussinesq assumption and the linear stress-strain relation it is more sound and better to use a non-linear stress-strain model.

#### 4.1.2 Transition Prediction

At first the too early transition on the suction side was thought to be caused by the above mentioned excessive production of turbulent energy in the stagnation region. However, since the transition location is not influenced at all by the Kato-Launder modification, this can not be the case. Previous tests [17] also show that the transition is not influenced by the inlet turbulence level. The conclusion is that the turbulence level in the free-stream does not affect the transition, which is in contradiction with the physics of the flow. The transition in the simulations seems to be caused by the geometry or the flow, and not by the turbulence. Similar trends, for the same case, have also been observed by other authors, using the Launder-Sharma model and a new non-linear three-equation model [8]. They also did simulations at different Reynolds numbers, and not even then did the transition point move!

A problem often encountered with the  $k-\omega$  models is that they are too sensitive to the free-stream value of  $\omega$ . This could potentially be used to tune a simulation. If the transition point is known in advance the inlet value of  $\omega$  can be adjusted until the correct location is obtained. This technique has been used by, for example, Chima [7]. Attempts to do the same here failed. In this case the transition point is quite independent of the free-stream value of  $\omega$ . Figure 4 shows that varying  $\omega$  at the inlet only affects the results close to the stagnation point. The same trend has also been observed with the transition  $k-\omega$  model and the  $k-\epsilon$  models. Included in figure 4 is also results obtained with different boundary conditions on  $\omega$  at the wall. Using  $k_R^+ = 5$  should give a hydraulically smooth surface, and further reducing  $k_R^+$  should not affect the results. The results obtained with  $k_R^+$  equal to 1 and 0.1 are also very similar, although a small influence can be seen in the leading edge region. This is probably due to numerical problems when  $\omega$  at the wall becomes too large.

## 4.2 Transonic Cascade

The second test-case is a transonic highly loaded cascade from the von Karman Institute of Fluid Dynamics (VKI). Heat-transfer measurements at many different operating conditions are available in Arts et. al. [2]. The case chosen here is referred to as Mur222. It

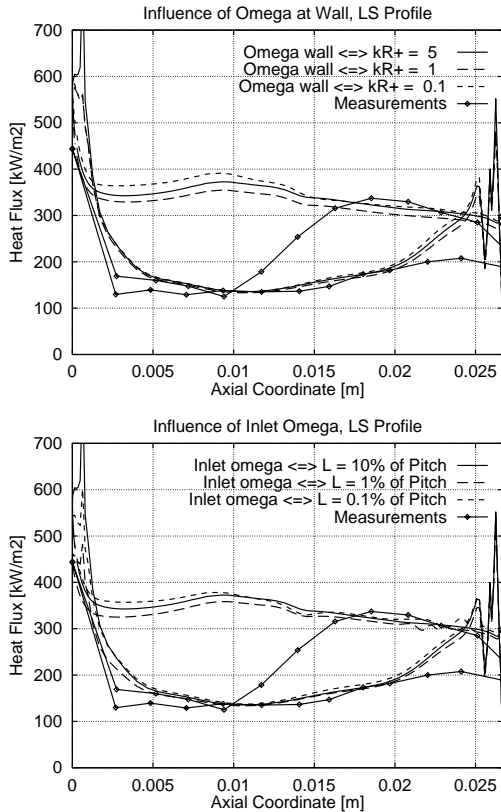


Figure 4: Wilcox Standard  $k - \omega$  model, Influence of  $\omega_{wall}$  and  $\omega_{inlet}$

has a high inlet turbulence level of 6%, an outlet Mach number of 1.1, and a chord Reynolds number based on outlet conditions of  $5 \cdot 10^5$ . On the suction side the boundary layer remains in a laminarizing state all the way back to the shock, which is located just at the trailing edge. Also on the pressure side the boundary layer is laminarizing, and no transition is visible. This makes it difficult to use a two-equation model for this case.

Figure 5 shows heat-transfer results obtained with all four turbulence models. Again only the Launder-Sharma model is able to capture a laminar region on the suction side. But the transition comes far too early, and gives the characteristic peak often predicted with the Launder-Sharma model.

All models have problems in the leading edge region. The Chien model gives a very high peak in the heat-transfer at the leading edge. The peak obtained with the Launder-Sharma model is significantly smaller and the  $k - \omega$  models are even better.

On the pressure side all models give quite good results, the Launder-Sharma model lies a bit below the measurements and the other three models are a bit above. But the overall trend is captured well with all

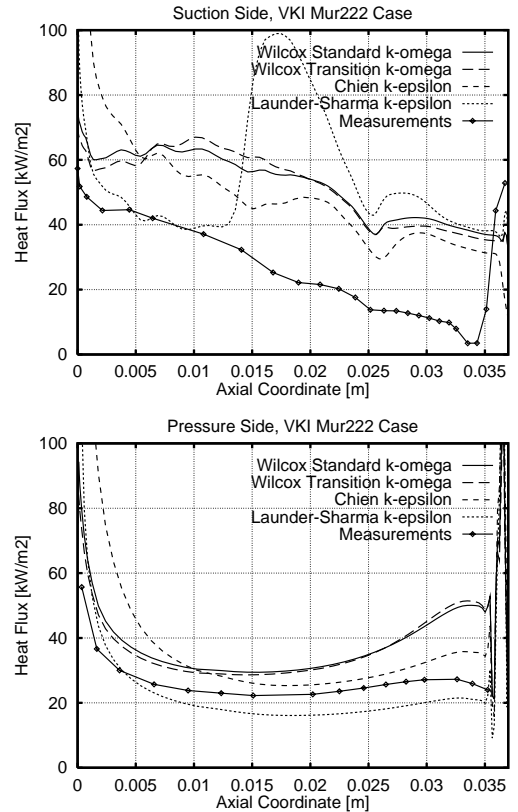


Figure 5: Heat Transfer, VKI Case Mur222

models.

### 4.3 Accuracy and Grid Independence

Error control is of fundamental importance in CFD. In lack of error estimates for the Navier-Stokes equations one is forced to compare with measurements. However, by demonstrating grid and scheme independence it is possible to rule out certain types of errors. A lot of effort has been put into ensuring that the results presented here are of high quality, and are representative of the turbulence models and not the numerics.

The experience regarding numerical errors for the cases presented here can be summarized in the following points:

- The grids used are sufficiently fine, and the results are grid independent. Figure 6 shows heat transfer results obtained for the subsonic “LS” case with two different grids and with two different convective schemes for  $k$  and  $\epsilon/\omega$ . The fine grid has about 20,000 nodes and the coarse grid 10,000. Only a very slight deviation can be seen close to the leading edge with the Launder-

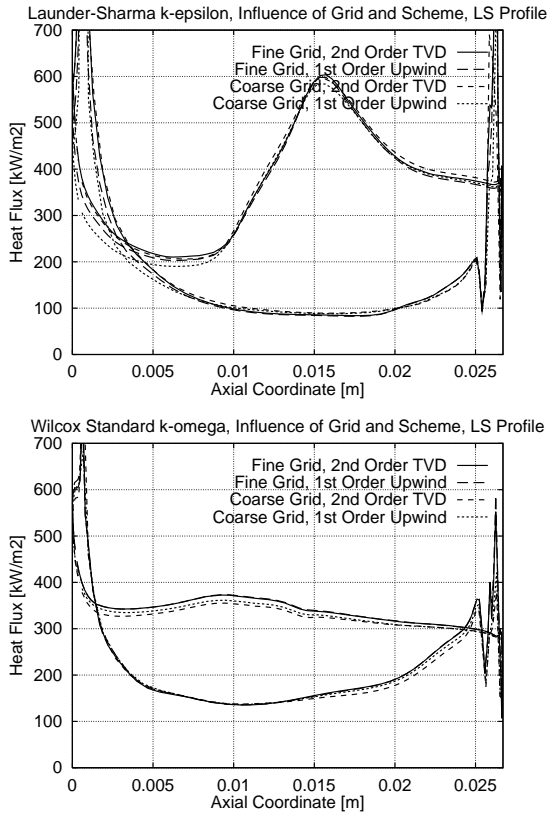


Figure 6: Influence of Grid and Scheme for the Turbulence Equations, “LS” Case

Sharma model, using the coarse grid and a first order upwind scheme. If not otherwise stated all simulations presented here have been made with the fine grid and the 2nd order TVD scheme.

- The leading-edge is the most sensitive region, and this is where numerical errors are first visible.
- Figure 7 shows heat-transfer results obtained with different grid spacings at the wall. When  $Y^+$  for the first cell is allowed to go up to 2 both the Launder-Sharma model and the standard  $k - \omega$  model show a clear deviation. The  $k - \omega$  model also shows a slight deviation for  $Y^+ < 0.2$  with the coarse grid. This is because with this grid the resolution of the outer parts of the boundary layers is not sufficient. This deviation is not present with the fine grid. For all models used it is important that the first cell is below  $Y^+ = 1$  in order to obtain grid independent results. Using an even finer spacing at the wall improves stability, and reduces problems with oscillations. The author recommends using  $Y^+ < 0.2$  for the first cell, with 5 cells below  $Y^+ = 1$ . With this distribution it is necessary

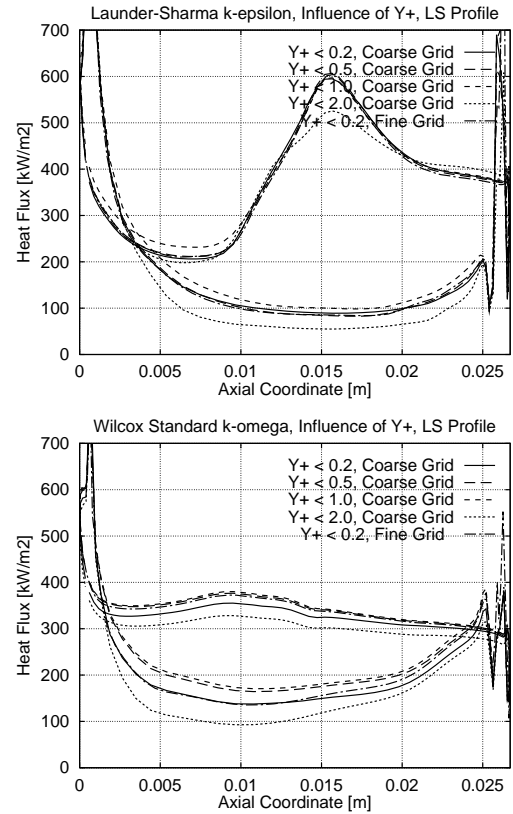


Figure 7: Influence of  $Y^+$  of First Cell, “LS” Case

to have at least 40 cells in the boundary layer. Most simulations presented here have around 60 cells in the boundary layer.

- It is often important to use double precision. With modern 64 bit computers this does not slow down the computations much, and all results presented here are in double precision.
- If the grid points along the blade surface are not smoothly distributed this immediately results in oscillations in the heat transfer. It is often not sufficient to use 3rd order interpolating splines in the grid generation. 5th order smoothed splines solves this problem.
- The  $k - \omega$  models generally have less numerical problems than the  $k - \epsilon$  models, although using a very low  $k_R^+$  or a high  $\omega_{inlet}$  can cause problems sometimes.
- The heat-transfer converges much slower than other properties of the flow-field. The best convergence criteria is to run until the heat-transfer does not change. This technique has been used for all cases. With a common density-variation

based residual this gives a residual decrease of more than 5 decades for all simulations presented here. The number of time-steps needed to obtain this is between 10.000 and 50.000.

## 5 Conclusions

It is evident from the results presented here that several problems remain to be solved before two-equation models can be used routinely in a Navier-Stokes code to predict turbine heat-transfer.

All models used are based on the Boussinesq assumption, and predict far too high turbulence levels in the stagnation region. The  $k - \epsilon$  models, and especially the Chien model, are much more influenced by this than the  $k - \omega$  models, and give a large peak in the heat-transfer. The  $k - \omega$  models are only affected in a very small region around the stagnation point.

None of the models tested are able to predict suction-side transition correctly. Only the Launder-Sharma model captures any laminar region. The predicted transition point is not influenced by the free-stream turbulence or the excessive production of turbulent energy in the leading edge region. It looks as if the transition is caused by the flow and the local blade geometry, and not by the external turbulence.

The heat-transfer in the turbulent part of the suction-side is predicted quite well by all models, although the Launder-Sharma model over-predicts it slightly.

The heat-transfer on the pressure side is also predicted quite well, except near the trailing edge where there sometimes is an unphysical rise in the heat-transfer. The Launder-Sharma model has a tendency to under-predict the pressure side heat-transfer slightly.

All models give oscillations at the separation point at the trailing edge. This is very difficult to avoid.

It is essential that the numerical quality of the solution is verified in some way. All models can give converged but incorrect results if the resolution of the boundary-layers is not sufficient.

The  $k - \omega$  models are easier to use numerically than the  $k - \epsilon$  models, and their results are as good or better. The  $k - \omega$  models also work better, but not well, in the leading edge region. No major difference has been found between the standard and the transition version of the  $k - \omega$  model.

## References

- [1] A. A. Ameri, P. M. Sockol, and R. S. R. Gorla. Navier-Stokes analysis of turbomachinery blade external heat transfer. *Journal of Propulsion and Power*, 8(2):374–381, 1992.
- [2] T. Arts, M. Lambert de Rouvriot, and A. W. Rutherford. Aero-thermal investigation of a highly loaded transonic liner turbine guide vane cascade. Technical Report 174, von Karman Institute for Fluid Dynamics, 1990.
- [3] D. A. Ashworth, J. E. LaGraff, D. L. Schultz, and K. J. Grindrod. Unsteady aerodynamic and heat transfer processes in a transonic turbine stage. *ASME Journal of Engineering for Gas Turbines and Power*, 107:1022–1030, 1985.
- [4] M. F. Blair. An experimental study of heat transfer in a large-scale turbine rotor passage. *ASME Journal of Turbomachinery*, 116(1):1–13, 1994.
- [5] R. J. Boyle. Navier-Stokes analysis of turbine blade heat transfer. *ASME Journal of Turbomachinery*, 113(3):392–403, 1991.
- [6] K.-Y. Chien. Predictions of channel and boundary-layer flows with a low-Reynolds number turbulence model. *AIAA Journal*, 20(1):33–38, 1982.
- [7] Rodrick V. Chima. A  $k - \omega$  turbulence model for quasi-three-dimensional turbomachinery flows. AIAA Paper 96-0248 and NASA TM-107051, 1996.
- [8] T. J. Craft, B. E. Launder, and K. Suga. The prediction of turbulent transitional phenomena with a non-linear eddy viscosity model. In *Proc. of the Engineering Foundation International Conference on Turbulent Heat Transfer, San Diego, March 1996*.
- [9] L. D. Daniels and W. B. Browne. Calculation of heat transfer rates to gas turbine blades. *International Journal of Heat and Mass Transfer*, 24(5):871–879, 1981.
- [10] D. J. Doorly and M. L. G. Oldfield. Simulation of the effect of shock wave passing on a turbine rotor blade. *ASME Journal of Engineering for Gas Turbines and Power*, 107:998–1006, 1985.
- [11] K. Dullenkopf and R. E. Mayle. The effect of an incident turbulence and moving wakes on laminar heat transfer in gas turbines. *ASME Journal of Turbomachinery*, 116(1):23–28, 1994.
- [12] K. Dullenkopf, A. Schultz, and S. Wittig. The effect of an incident wake conditions on the mean heat transfer of an airfoil. *ASME Journal of Turbomachinery*, 113:412–418, 1991.

- [13] A. Favre. Equations des gaz turbulents compressibles. *Journal de Mecanique*, 4(3):361–390, 1965.
- [14] L. D. Hylton, M. S. Mihelc, E. R. Turner, D. A. Nealy, and R. E. York. Analytical and experimental evaluation of the heat transfer distribution over the surfaces of turbine vanes. NASA CR-168015, 1983.
- [15] M. Kato and B. E. Launder. The modeling of turbulent flow around stationary and vibrating square cylinders. In *Proc. 9th Symposium on Turbulent Shear Flows, Kyoto*, pages 10.4.1–10.4.6, August 1993.
- [16] Jonas Larsson. Numerical simulation of turbine blade heat transfer. Licentiate Thesis, Department of Thermo and Fluid Dynamics, Chalmers University of Technology, Gothenburg, Sweden (Also available on the Internet at <http://www.tfd.chalmers.se/~jola/>), 1996.
- [17] Jonas Larsson, Lars-Erik Eriksson, and Ulf Håll. External heat transfer predictions in supersonics turbines using the Reynolds averaged Navier-Stokes equations. In *Proc. 12:th ISABE Conference, Melbourne*, volume 2, pages 1102–1112. (Copies distributed by AIAA), September 1995.
- [18] B. E. Launder and B. I. Sharma. Application of the energy-dissipation model of turbulence to the calculation of flow near a spinning disc. *Letters in Heat and Mass Transfer*, 1(2):131–138, 1974.
- [19] P. K. Maciejewski and R. J. Moffat. Heat transfer with very high free-stream turbulence: Part i and ii. *ASME Journal of Heat Transfer*, 114:827–839, 1992.
- [20] P. J. Magari and L. E. LaGraff. Wake-induced unsteady stagnation-region heat transfer measurements. *ASME Journal of Turbomachinery*, 116(1):29–38, 1994.
- [21] J. H. Nicholson, A. E. Forest, M. L. G. Oldfield, and D. L. Schultz. Heat transfer optimised turbine rotor blades - an experimental study using transient techniques. ASME Paper 82-GT-304, 1982.
- [22] Virendra C. Patel, Wolfgang Rodi, and Georg Scheuerer. Turbulence models for near-wall and low Reynolds number flows: A review. *AIAA Journal*, 23(9):1308–1319, 1985.
- [23] K. V. Rao, R. A. Delaney, and M. G. Dunn. Vane-blade interaction in a transonic turbine. *Journal of Propulsion and Power*, 10(3):305–317, 1994.
- [24] K. A. Thole and D. G. Bogard. Enhanced heat transfer due to high free-stream turbulence. *ASME Journal of Turbomachinery*, 117:418–424, 1995.
- [25] D. Vandromme. Turbulence modeling for compressible flows and implementation in Navier-Stokes solvers. von Karman Institute for Fluid Dynamics, Lecture Series 1991-02, Introduction to the Modeling of Turbulence, 1991.
- [26] David C. Wilcox. Reassessment of the scale determining equation for advanced turbulence models. *AIAA Journal*, 26(11):1299–1310, 1988.
- [27] David C. Wilcox. *Turbulence Modeling for CFD*. DCW Industries, Inc., La Cañada, California, 1993.
- [28] David C. Wilcox. Simulation of transition with a two-equation turbulence model. *AIAA Journal*, 32(2):247–255, 1994.
- [29] C. J. Yap. *Turbulent Heat and Momentum Transfer in Recirculating and Impinging Flows*. PhD thesis, Faculty of Technology, University of Manchester, 1987.
- [30] Frederick C. Yeh, Steven A. Hippensteele, James G. Van Fossen, and Philip E. Poinatte. High Reynolds number turbulence effects on turbine heat transfer. *Journal of Propulsion and Power*, 10(6):868–875, 1994.